W-band Up-conversion Module for Passive Millimeter-wave Imager Using Folded Thin-film Lithium Niobate Modulators

Shouyuan Shi*[ab], Peng Yao[b], Chris Schuetz[b], Timothy Creazzo[b], Xiaofeng Zhu[a], and Dennis W. Prather[ab]

[a] Department of Electrical and Computer Engineer, University of Delaware, Newark, DE 19716, USA;
[b] Phase Sensitive Innovations, Newark, DE 19713, USA;
*sshi@udel.edu

ABSTRACT

This paper presented to leverage thin-film Lithium Niobate (TFLN) technologies to develop high-speed high-efficiency electro-optic (EO) phase modulator for efficient up-conversion process in the millimeter wave (mmW) regime for the applications to passive mmW imaging applications. Compared with bulk LN modulators, TFLN modulators offer stronger EO interaction owing to tighter RF and optical mode sizes, thereby demonstrating significant modulation enhancement, i.e., >50×. Various TFLN modulator designs, including hybrid SiN and ridge-etched TFLN, on the quartz and silicon substrates are investigated. Additionally, tighter optical waveguide bending allows single-end optical interface on one side and RF feed on the other side, thereby leading to more compact device packaging and easier system integration. Furthermore, capacitively loaded travelling wave electrodes (CL-TWE) are developed for better RF and optical index matching < 0.002, and lower RF loss of < 0.8 dB/GHz^{-1} for better conversion efficiency in W-band. The fabricated TFLN modulators on silicon handle are integrated with the RF module, and the packaged module was experimentally verified that the TFLN-based module demonstrates significantly improved performance, > 8 dB in EO conversion efficiency, ~ 50% reduction in packaging size when packaged as a multiple channel blade.

Keywords: Passive millimeter wave (PmmW) imaging, W-band, Up-conversion Module, Thin-film Lithium Niobate (TFLN) Modulator, Folded EO modulator, Modulator packaging

1. INTRODUCTION

Real-time and video-rate passive millimeter wave (pmmW) imagery has received tremendous interest owing to its ability to see-though obstacles, operate all time and all-weather conditions. Over the last decade, photonically assisted pmmW imagers have been developed, demonstrating unprecedent image performance of sensitivity of < 0.5 K and angular resolution of < 0.5^{o} [1], [2]. The photonic-based imager uses high-speed (~100GHz) electro-optic (EO) modulators [3] to convert received mmW radiation into optical sidebands , and then relaunching as an array to form two-dimensional images using a simple Fourier optic lens [4]. Such a technique offers many advantages over traditional imaging techniques, such as lightweight and low-loss fiber optics for signal routing, elimination of bulky mmW local oscillator (LO), and room-temperature operation. To compensate for extremely low power black body radiation in mmW region, multiple stages of low noise amplifiers (LNAs) with >60dB gain are typically used, which impose significant challenges in RF packaging. To ease RF integration, advanced modulator development with *enhanced modulation efficiency* becomes particularly important.

Over the last decade, tremendous effort has been made to develop high-speed bulk LN phase modulators have been tested up to 300 GHz with excellent optical response [3]. However, such an EO modulator suffers from large device size and insufficient modulation efficiency for pmmW imaging applications. To further improve EO modulation efficiency, we have been working on the development of TFLNOI modulators [5], [6]. Compared with the bulk optical LN modulators, much smaller optical and RF mode sizes developed in TFLNOI lead to a stronger field concentration and better mode overlap between the optical and RF signals, thereby demonstrating significant modulation enhancement and reduced device footprint.

Terahertz, RF, Millimeter, and Submillimeter-Wave Technology and Applications XVIII,
edited by Laurence P. Sadwick, Tianxin Yang, Proc. of SPIE Vol. 13365,
133650T · © 2025 SPIE · 0277-786X · doi: 10.1117/12.3043854

2. HIGH-SPEED FOLDED TFLNOI PHASE MODULATOR DEVELOPMENT

By leveraging Thin-Film Lithium Niobate on Insulator (TFLNOI) technologies, we have developed compact, high-efficiency, high-speed, and low insertion loss optical modulators. Modulation efficiency of EO modulators can be maximized owing to highly confined optical mode profiles, i.e., in an order of about 2×3 um^2, which is >10× smaller than the conventional diffused optical waveguides in the bulk LNB substrates. As a result, the RF electrodes, i.e., coplanar waveguide, can be patterned with a much smaller gap between the electrodes, which leads to significant RF field concentration between the RF electrodes where the optical waveguide resides. Over time, many different optical waveguides, including hybrid silicon nitride (SiN) strip loaded waveguides and ridge-etched TFLN waveguides, have been researched on different handle substrates, such as silicon and quartz [5], [7], [8], [9]. Parametric studies of these optical waveguides are investigated to find optimal dimensions for best device performance, including low $V_\pi L$ and low optical loss. In addition, to achieve a wide RF bandwidth, various RF electrode structures are designed to provide a low RF propagation loss and good index matching between the RF and optical modes at high RF frequencies, up to 100 GHz.

The hybrid SiN strip loaded TFLN defines the optical waveguides by patterning the SiN strip on the uniform TFLN substrate, which offers advantages of lower optical propagation loss and easy coupling to the optical fibers. In contrast, a ridge etched TFLN modulator offers improved $V_\pi L$ due to smaller optical mode size and better confinement factor in TFLN [8]. Figure 1(a) shows the cross-section of the ridge etched TFLN MZI modulator, in which the TFLN film has a thickness of 600 nm, and etched ridge width and depth are W_{rg} = 1000 nm and H_{rg} = 300 nm, respectively. Such an optical waveguide supports single mode operation at a wavelength of 1.55 um and provides optical mode confinement in TFLN > 85%. Additionally, to minimize potential metal absorption of the guided mode due to the presence of the driving electrodes, a thin buffer oxide layer can be deposited on the TFLN before patterning of the electrodes. Figure 1(b) and (c) show the RF and optical modes with the electrode gap of 4 μm. Strong electric field, 0.78 V/μm, can be established when 1 volt is applied across the coplanar waveguide (CPW). Based on model overlap between the RF and optical modes, the extracted $V_\pi L$ is 1.94 V·cm, leading to V_π < 1 V if a 20 mm modulator is considered.

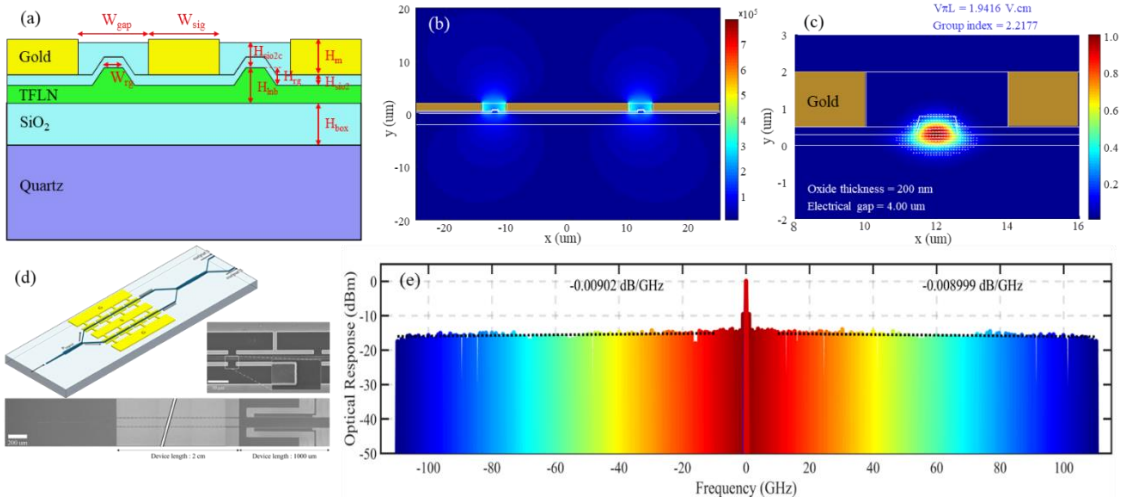

Figure 1. (a) Cross-sectional view of ridge etched TFLN modulator on quartz substrate. Simulated (b) RF and (c) optical guided mode of a ridged etched TFLN modulator. (d) Layout and SEM pictures of the dual-output MZI modulator. (e) Measured optical sideband response of the fabricated ridge-etched TFLN MZI modulator.

For mmW modulator development, low-loss, impedance and velocity matched RF electrodes are critical. To this end, capacitively loaded traveling wave electrodes (CL-TWEs) are designed for the TFLN platforms for both silicon and quartz handles. Parameters of the electrode segments were studied using HFSS in terms of CPW effective index, impedance and modulation efficiency. The theoretical results were compared with the experimental results, where good matches were obtained. Significant RF propagation loss improvement was achieved using the CL-TWE compared to the conventional CPW. The optimized CL-TWEs are fabricated and characterized, demonstrating RF loss of -8 dB at 100 GHz for a 2cm long modulator. The final layout and fabricated device of the dual output MZI modulator is illustrated in Fig. 1(d). The fabricated device is characterized to demonstrate the DC V_π of about 1 V and ultrawideband frequency response. The measured optical sideband response over the frequency up to 220 GHz is shown in Fig. 1(e), demonstrating the 3dB EO bandwidth of 125 GHz.

On the other hand, due to tightly confined optical mode and high index contrast of the optical guided mode, TFLN modulators allow sharp bending of the optical waveguides [10]. Benefiting from such a property, as shown in Fig. 2, a folded modulator configuration was developed, where both the input and output fiber ports are located on the same end of the modulator chip. A thin, compact modulator package was developed for conceptional demonstration for a dense mmW imager systems or other phased array systems.

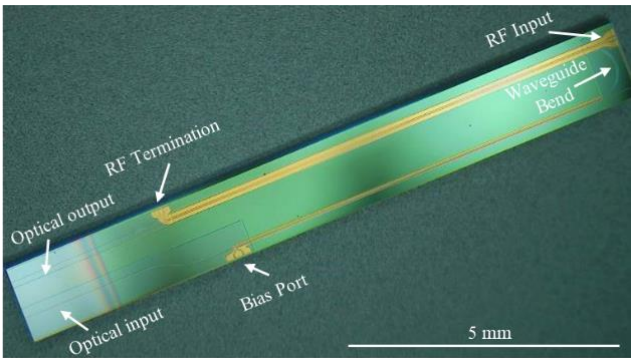

Figure 2. Fabricated folded TFLN modulator with the optical input and output at the left side and RF input at the right side.

To characterize the modulator device for pmmW imaging applications, modulator conversion efficiency is introduced. Under the small signal approximation, the modulated optical sideband can be determined by $P_{sb} = \eta_{mod} P_{RF} P_{opt}$, in which $\eta_{mod}(f)$ is the modulator conversion efficiency for both phase and MZI modulators, given by:

$$\eta_{mod(f)} = \begin{cases} \frac{\pi^2 Z_{mod}}{2V_\pi^2(f)} & \text{for phase modulator} \\ \frac{\pi^2 Z_{mod}}{8V_\pi^2(f)} & \text{for push-pull MZI modulator} \end{cases},$$

where Z_{mod} is the RF impedance of the modulator, and $V_\pi(f)$ is the frequency dependent half-wave voltage. Conversion efficiency can be used as modulator performance metric in the applications to the imaging system.

Improved modulation responses up to 100 GHz of the TFLN modulators developed on various material platforms demonstrate significant enhancement in up-conversion efficiency when used in passive millimeter wave imaging systems. Performance comparison of various devices is listed in Table I. The improved up-conversion efficiency dramatically reduces the RF gain requirement, i.e., less than 30 dB gain, essentially relaxing the RF and optical integration complexity for low system SWaP-C.

Table 1. Performance comparison of various modulator devices

Modulator Device	**Device length**	**Modulator Type**	**Mode Confinement**	$V_\pi L$	**DC V_π**	**Optical Loss**	η_{mod} (L_{dev} = 20 cm)
Bulk LN [3]	20 mm	Phase	99%	16 V·cm	8 V	< 0.1 dB/cm	3.8 W^{-1}
Hybrid SiN-TFLN Mod w/QZ [our work]	23 mm	MZM	65.4%	2.7 V·cm	1.2 V	< 6 dB/cm	33.8 W^{-1}
CL-TWE TFLN Mod W/QZ [9]	6 mm	MZM	>90%	1.62 V·cm	2.7 V	0.66 dB/cm	94.0 W^{-1}
CL-TWE TFLN Mod W/QZ [8]	20 mm	MZM	89.5%	2.0 V·cm	1.0 V	0.74 dB/cm	61.7 W^{-1}
TFLN Mod w/Si removal [11], [12]	15 mm	MZM	>90%	2.2 V·cm	1.5 V	0.15 dB/cm	51.0 W^{-1}
Hybrid TFLN Mod w/Si [7]	11 mm	MZM	69.5%	3.3 V·cm	3.0 V	0.65 dB/cm	22.7 W^{-1}

3. W-BAND TFLN MODULTOR PACKAGING AND CHARCATERIZATIONS

The folded modulator design, illustrated in Fig. 2, allows an ultimate up-conversion module configuration, in which the driving RF signal feeds from one side, while the optical input and output signals are coupled from the other side of the TFLN chip. With successful development of thin film $LiNbO_3$ modulator on the quartz and silicon handles, we completed the package design of the TFLN for W-band passive millimeter wave imaging applications. To this end, we fabricated the folded modulator chip on a 300nm LN, silicon handle LNOI wafer, where we included both a high-speed EO modulator for RF input and a low-speed EO modulator for bias control. We also worked out the fiber integration process and demonstrated a low fiber-to-fiber insertion loss, <7dB, for the WR10 modulator prototype. Over 100GHz operational bandwidth and ~1.5 W^{-1} conversion efficiency was measured. Combining WR10 transition and folded modulator designs, we designed, fabricated, integrated, and characterized a WR10 TFLN phase modulator package, as shown in Fig. 4(a).

To realize efficient transition from a W-band waveguide to the modulator, a thin ceramic probe is introduced between the modulator and WR10 rectangular waveguide. As shown in the inset in Fig. 3(a), the ceramic probe chip consists of a V-dipole probe, a coplanar strip line, a coplanar waveguide, and a transition between two transmission lines. The ceramic probe chip is placed in the end of the WR10 waveguide and bonded to TFLN chip through low-profile wirebonds. To feed the V-dipoles with a conventional CPW, a transition from the CPW to a slot line is developed, in which one gap of the CPW is connected to a slot line that feeds the V dipole probe, and the other gap is terminated with a radial stub. At the transition, high profile wire bonds are added to shorten the ground planes to minimize the radiation and scattering. On the other hand, the ceramic probe is placed at the end wall of the WR10 waveguide. The simulated S parameters are shown in Fig. 3(b). The return loss over the frequency band of 75 GHz to 110 GHz is less than -10 dB and the transmission loss is less than -1.0 dB. The designed package was machined for probe testing, consisting of a top housing and a bottom housing. The housings are bolted together to form the input WR10 waveguide. The top housing is, however, terminated right above the end of the transition probe chip such and the probe chip was epoxied to the bottom housing, followed by wire-bonding to connect the two grounds. The test structure assembly was probe tested using our PNA and a probe station. A WR10 waveguide was used as the input and a 100GHz GSG probe was used to measure the transmitted RF power. The GSG probe was landed on the transition probe. The test results are summarized in Fig. 3(b).

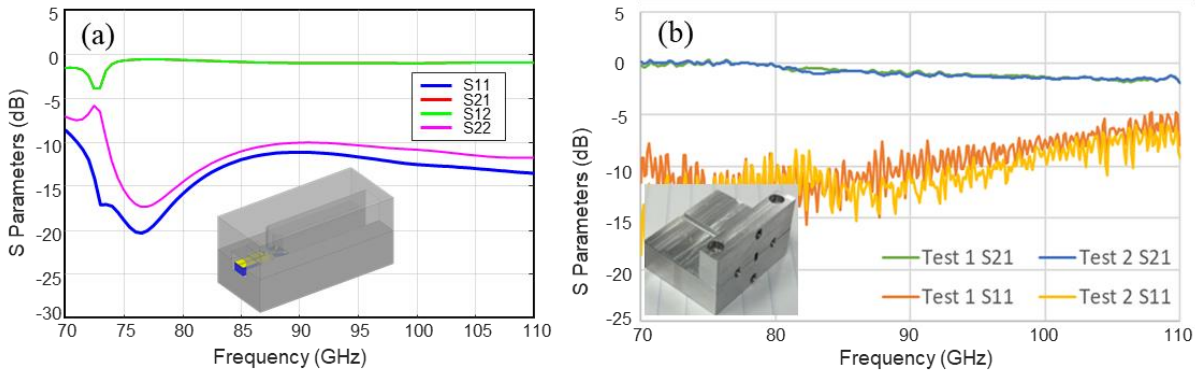

Figure 3. (a) Simulated S parameters of the probe transition for W0band modulator packaging. (b) Measured S-parameters of the transition probe chips.

Based on the above transition probe chip design, we have designed a W-band LNOI modulator prototype package for device demonstration, as shown in Fig. 4. Following the WR10 input, a TFLN modulator on silicon handle is placed against the transition probe chip, where the CPWs on the probe chip and the CPWs on the modulator chip are wire-bonded using very low-profile gold wires. Due to the high index contrast provided by the LNOI waveguide, the input optical waveguide is folded on the LNOI chip such that both input and output waveguides are coupled to the corresponding fibers on the same VGA. The customized VGA consists of two short UHNA fibers at the modulator side and two standard PM fibers at the output port side. A customized fiber stress relief boot is used to manage the fiber pigtail. For imager application, DC bias is needed for active phase control. The DC bias signal is applied through a 1×2 pogo pin array mounted at the bottom of the package.

The WR10 TFLNOI modulator package was tested using our modulator characterization setup, and ~6.6 dB fiber-to-fiber insertion was measured. Fig. 3(c) shows the normalized sidebands measured from 61 GHz to 110 GHz, demonstrating significant sideband power improvement at low frequencies compared to our bulk LN modulator products. However, faster

sideband roll-off, ~5 dB from 70 GHz to 100 GHz, was also observed. This was caused by two reasons. First, the index matching between RF, 2.2, and optical, 2.4, modes was not ideal, which led to a wavy pattern in the measured sidebands. Second, the RF loss at 110 GHz was ~7 dB higher than that at 70 GHz, which accounted for ~3.5 dB sideband power roll-off.

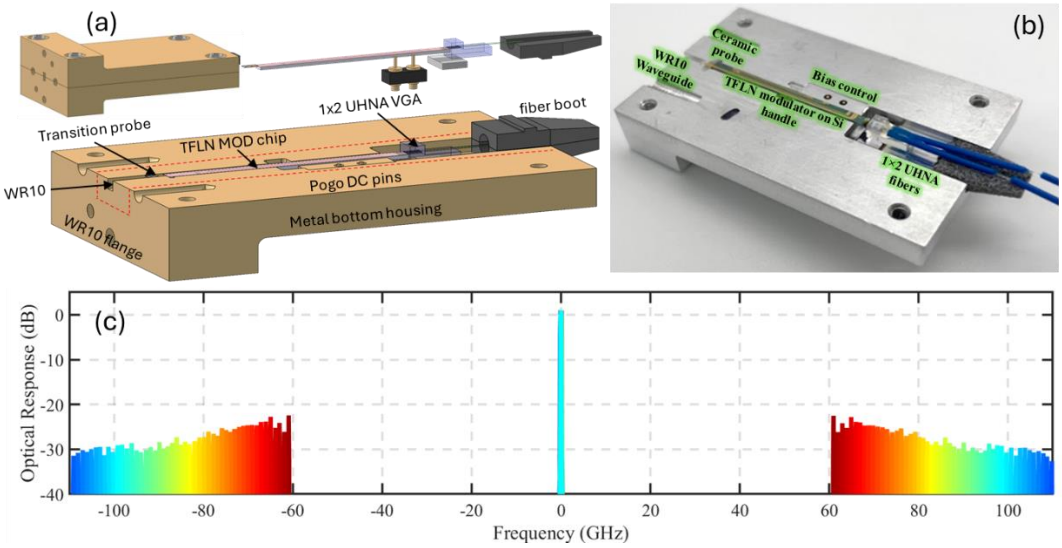

Figure 4. (a) LNOI modulator packaging design. (b) Packaged WR10 fed folded TFLN phase modulator. (c) Normalized sidebands of the WR10 LNOI modulator package.

To further improve EO modulation efficiency at higher RF frequences, TFLN on Si handle is replaced with TFLN on quartz handle owing to its much lower dielectric loss than silicon. On the other hand, to realize accurate match between the RF index and optical group index of 2.24 for wide band operation, capacitively loaded traveling wave electrodes (CL-TWE) are developed. Packaging of such a TFLN modulator will be future effort to further improve the development of passive mmW imaging systems.

4. CONCLUSIONS

This paper presented high-speed high-efficiency electro-optic phase modulators based on thin-film Lithium Niobate for efficient up-conversion process at the millimeter wave regime. The developed TFLN modulators demonstrated significant modulation enhancement, >50×, and reduced device footprint owing to single-end optical feed. Furthermore, capacity loaded electrodes are developed for better RF and optical index match, and lower RF loss for better conversion efficiency in W band. The hybrid SiN-TFLN modulators on silicon handle were fabricated and integrated with the RF module, and the packaged module was experimentally verified that the TFLN-based module demonstrates significantly improved performance, > 8 dB in EO conversion efficiency, ~ 50% reduction in packaging size when packaged as a multiple channel blade.

REFERENCES

[1] C. Schuetz *et al.*, "Realization of a video-rate distributed aperture millimeter-wave imaging system using optical upconversion," presented at the SPIE Defense, Security, and Sensing, D. A. Wikner and A. R. Luukanen, Eds., Baltimore, Maryland, USA, May 2013, p. 87150I. doi: 10.1117/12.2016138.

[2] D. W. Prather *et al.*, "Millimeter-Wave and Sub-THz Phased-Array Imaging Systems Based on Electro-Optic Up-Conversion and Optical Beamforming," *IEEE J. Select. Topics Quantum Electron.*, vol. 29, no. 5: Terahertz Photonics, pp. 1–14, Sep. 2023, doi: 10.1109/JSTQE.2023.3306953.

[3] J. Macario, Peng Yao, R. Shireen, C. A. Schuetz, Shouyuan Shi, and D. W. Prather, "Development of Electro-Optic Phase Modulator for 94 GHz Imaging System," *J. Lightwave Technol.*, vol. 27, no. 24, pp. 5698–5703, Dec. 2009, doi: 10.1109/JLT.2009.2035641.

[4] D. W. Prather *et al.*, "Fourier-Optics Based Opto-Electronic Architectures for Simultaneous Multi-Band, Multi-Beam, and Wideband Transmit and Receive Phased Arrays," *IEEE Access*, vol. 11, pp. 18082–18106, 2023, doi: 10.1109/ACCESS.2023.3244063.
[5] P. Kharel, C. Reimer, K. Luke, L. He, and M. Zhang, "Breaking voltage–bandwidth limits in integrated lithium niobate modulators using micro-structured electrodes," *Optica*, vol. 8, no. 3, p. 357, Mar. 2021, doi: 10.1364/OPTICA.416155.
[6] A. J. Mercante, S. Shi, P. Yao, L. Xie, R. M. Weikle, and D. W. Prather, "Thin film lithium niobate electro-optic modulator with terahertz operating bandwidth," *Opt. Express*, vol. 26, no. 11, p. 14810, May 2018, doi: 10.1364/OE.26.014810.
[7] S. P. Nelan *et al.*, "Ultra-High Extinction Dual-Output Thin-Film Lithium Niobate Intensity Modulator," *IEEE Access*, vol. 10, pp. 100300–100311, 2022, doi: 10.1109/ACCESS.2022.3207764.
[8] X. Zhu *et al.*, "Ultra Wideband Dual-Output Thin Film Lithium Niobate Intensity Modulator," *IEEE J. Select. Topics Quantum Electron.*, vol. 30, no. 4: Adv. Mod. and Int. beyond Si, pp. 1–13, Jul. 2024, doi: 10.1109/JSTQE.2024.3388324.
[9] X. Liu *et al.*, "Capacitively-Loaded Thin-Film Lithium Niobate Modulator With Ultra-Flat Frequency Response," *IEEE Photon. Technol. Lett.*, vol. 34, no. 16, pp. 854–857, Aug. 2022, doi: 10.1109/LPT.2022.3178214.
[10] S. Nelan *et al.*, "Compact thin film lithium niobate folded intensity modulator using a waveguide crossing," *Opt. Express*, vol. 30, no. 6, p. 9193, Mar. 2022, doi: 10.1364/OE.453050.
[11] X. Liu *et al.*, "Sub-terahertz bandwidth capactively-loaded thin-film lithium niobate electro-optic modulators based on an undercut structure," *Opt. Express*, vol. 29, no. 25, p. 41798, Dec. 2021, doi: 10.1364/OE.442091.
[12] G. Chen *et al.*, "High performance thin-film lithium niobate modulator on a silicon substrate using periodic capacitively loaded traveling-wave electrode," *APL Photonics*, vol. 7, no. 2, p. 026103, Feb. 2022, doi: 10.1063/5.0077232.
[13] S. P. Nelan *et al.*, "Integrated Lithium Niobate Intensity Modulator on a Silicon Handle With Slow-Wave Electrodes," *IEEE Photon. Technol. Lett.*, vol. 34, no. 18, pp. 981–984, Sep. 2022, doi: 10.1109/LPT.2022.3197085.